

Biologically induced initiation of Neoproterozoic snowball-Earth events

Eli Tziperman^{a,1}, Itay Halevy^b, David T. Johnston^a, Andrew H. Knoll^a, and Daniel P. Schrag^a

^aDepartment of Earth and Planetary Sciences, Harvard University, 20 Oxford Street, Cambridge, MA 02138; and ^bDivision of Geological and Planetary Sciences, California Institute of Technology, MC 100-23, 1200 East California Boulevard, Pasadena, CA 91125

Edited by Timothy W. Lyons, University of California, Riverside, CA, and accepted by the Editorial Board July 12, 2011 (received for review November 11, 2010)

The glaciations of the Neoproterozoic Era (1,000 to 542 MyBP) were preceded by dramatically light C isotopic excursions preserved in preglacial deposits. Standard explanations of these excursions involve remineralization of isotopically light organic matter and imply strong enhancement of atmospheric CO₂ greenhouse gas concentration, apparently inconsistent with the glaciations that followed. We examine a scenario in which the isotopic signal, as well as the global glaciation, result from enhanced export of organic matter from the upper ocean into anoxic subsurface waters and sediments. The organic matter undergoes anoxic remineralization at depth via either sulfate- or iron-reducing bacteria. In both cases, this can lead to changes in carbonate alkalinity and dissolved inorganic pool that efficiently lower the atmospheric CO₂ concentration, possibly plunging Earth into an ice age. This scenario predicts enhanced deposition of calcium carbonate, the formation of siderite, and an increase in ocean pH, all of which are consistent with recent observations. Late Neoproterozoic diversification of marine eukaryotes may have facilitated the episodic enhancement of export of organic matter from the upper ocean, by causing a greater proportion of organic matter to be partitioned as particulate aggregates that can sink more efficiently, via increased cell size, biomineralization or increased C:N of eukaryotic phytoplankton. The scenario explains isotopic excursions that are correlated or uncorrelated with snowball initiation, and suggests that increasing atmospheric oxygen concentrations and a progressive oxygenation of the subsurface ocean helped to prevent snowball glaciation on the Phanerozoic Earth.

carbon isotopes | CO₂

Between 750 and 580 million years (My) ago, the Earth experienced multiple ice ages, two of which deposited glaciogenic sediments in equatorial seas (1–3). These “snowball” glacial records have no equivalent in younger successions, and, indeed, there is little evidence for continental ice sheets of any kind in the preceding 1,500 My. A runaway ice albedo can lead to global glaciation once sea ice crosses a critical latitude of about 30 to 40°. However, the initial trigger that led to a critical extent of sea ice cover is far from obvious, although many potential drivers have been proposed (4). Solar luminosity was 7% lower than at present, yet this by itself cannot constitute the needed trigger because luminosity was even lower during earlier periods when no glaciation is recorded. The stratigraphic distribution of glaciogenic rocks thus presents two questions of timing. First, why are unusually severe ice ages limited to the observed interval of later Neoproterozoic time? And second, what initiated discrete and repeated episodes of global glaciation within this interval?

Tectonic arguments have been proposed to explain the first of these questions via the triggering of carbon cycle feedbacks. Later Neoproterozoic rifting, supercontinent breakup and low-latitude continents provided mechanisms for enhanced organic carbon burial and, hence, drawdown of atmospheric CO₂ (3–6). Neoproterozoic concentration of highly reflecting continental area near the equator reduced the absorption of solar radiation (2), while also eliminating the negative feedback between CO₂ abundance and the rate of chemical weathering, which would otherwise

occur via the glaciation of higher-latitude continents (4). Finally, low-latitude continents might strengthen chemical weathering by exposing continental areas to high precipitation rates and high temperature (3). However, these tectonic arguments do not explain what prevented the Earth from plunging into another snowball as soon as one was over, given that continental drift is slow relative to the time scale of the carbon cycle feedbacks being triggered.

The two most extensive Neoproterozoic glaciations were preceded by a distinct excursion of carbon isotopic values in carbonate rocks (the pre-Sturtian Islay anomaly and the pre-Marinoan Trezona anomaly); in each case, $\delta^{13}\text{C}$ declined more than 10 permil, from strongly positive values broadly characteristic of early Neoproterozoic carbonates (7, 8) to negative values rarely observed in rocks of any age. The duration of the preglaciation isotopic excursions is not well constrained, but the Trezona anomaly in Namibia, for example, is estimated from tectonic subsidence rates to have come and gone on the order of 0.5–1 My (9). It has been argued that the excursions were caused by a decrease in the organic carbon burial fraction (3), a decrease in productivity relative to carbonate deposition due to ocean cooling (3), a rapid turnover of poorly ventilated deep oceans (10), or the oxidation of a large organic carbon reservoir (11). Although all of these mechanisms could, in principle, cause $\delta^{13}\text{C}$ values to decline, most could enhance atmospheric CO₂, making them unlikely triggers for glaciation.

In some Neoproterozoic successions, the isotopic excursions are recorded in carbonate rocks but not in associated organic carbon (11–13). However, recent evidence (14) suggests that $\delta^{13}\text{C}$ of the organic and inorganic pools covaried through at least some of these excursions. Although it is possible that the dramatic presnowball $\delta^{13}\text{C}$ excursions (8) are not related to the glaciation or may even be diagenetic (15–17), the proximity of the two in several geological records suggests that we must consider the possibility that they are related. If related to the snowball events, the $\delta^{13}\text{C}$ excursions may indicate that the marine biosphere underwent major changes prior to snowball events. In order to explain both a snowball initiation and the preglaciation isotopic signal with a single mechanism, Schrag et al (4) considered a slow but sustained release of methane from isotopically light, deep ocean methane clathrates.

Here, we consider an alternative possibility, that the snowball events and isotopic excursions were both triggered by biological changes involving marine microorganisms via anaerobic remineralization of organic matter. Motivated by recent findings (11, 18, 19), we also present variants of the scenario in which glaciation could be triggered by the marine biosphere without producing an

Author contributions: E.T. designed research; E.T., I.H., D.T.J., A.H.K., and D.P.S. performed research; and E.T., I.H., D.T.J., A.H.K., and D.P.S. wrote the paper.

The authors declare no conflict of interest.

This article is a PNAS Direct Submission. T.W.L. is a guest editor invited by the Editorial Board.

¹To whom correspondence should be addressed. E-mail: eli@eps.harvard.edu.

This article contains supporting information online at www.pnas.org/lookup/suppl/doi:10.1073/pnas.1016361108/-DCSupplemental.

isotopic excursion and vice versa. The mechanism, although necessarily speculative, may explain why snowball events occurred in the Neoproterozoic but not thereafter, addresses the time scale between events, seems consistent with snowball-related geochemical observations, and makes several testable predictions.

An Overview of the Snowball Initiation Scenario

First, we consider attempts to explain preglacial isotopic excursions by a net aerobic remineralization of isotopically light organic matter. Fig. 1 shows such a scenario (using the model described in *Materials and Methods* and the *SI Appendix*). The scenario assumes a temporary drop in oxygenic primary production while aerobic remineralization proceeds unchanged (Fig. 1A). The pool of dissolved organic carbon (DOC) consequently shrinks while the dissolved inorganic carbon (DIC) pool grows (Fig. 1B), and the isotopic composition of both becomes significantly lighter (Fig. 1B). However, as a result of the increased DIC pool, atmospheric $p\text{CO}_2$ rises dramatically (Fig. 1C), preventing glaciation and, therefore, seemingly inconsistent with the observed record.

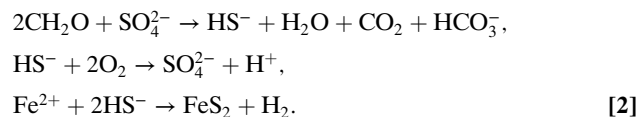
There are many indications that the oxygen minimum zone of Neoproterozoic oceans tended toward anoxia (20, 21). With this in mind, we consider a steady state of ocean biogeochemistry, with oxygenic upper ocean primary production by cyanobacteria and algae balanced largely by aerobic remineralization within the surface ocean mixed layer. A (small) net export production flux would maintain subsurface water-column anoxia by consuming dissolved oxygen mixed into the subsurface ocean from oxygenated surface water. Most of the organic matter would be contained within the upper oxygenated ocean in both dissolved form and suspended particulate form (e.g., cyanobacteria cells) that tends to remain in the upper ocean because of its relative

buoyancy; both forms are referred to together below as DOC. Further consider the possibility that at some point an increase in this export rate sends an enhanced flux of organic matter into anoxic subsurface waters and sediments, where it could be remineralized to dissolved inorganic carbon via anaerobic respiration by either sulfate reducing bacteria or iron-reducing bacteria, or buried.

Enhanced export production causes partially oxygenated subsurface ocean layers to be stripped of oxygen by the enhanced aerobic remineralization of sinking organic matter. This extends the depth range through which anoxic conditions dominate and may, therefore, reduce both oxygenic production and aerobic remineralization. As we will see shortly, this combination can lead to a reduction of atmospheric $p\text{CO}_2$ as well as a carbon isotopic signal consistent with the observed presnowball excursions. To appreciate this, examine now how these processes affect the marine carbonate system. Production and remineralization in the upper ocean may be represented by



Next, the anoxic remineralization of organic matter via sulfate (SO_4^{2-}) reduction leads to the formation of sulfide (H_2S , or in its dissociated form, HS^-). Sulfide can either diffuse toward the oxygenated upper ocean and be oxidized back into sulfate, or react with Fe^{2+} to form pyrite. These three processes may be represented by



Sulfate reduction can take place in anoxic subsurface water, although the sediments are a more likely site because of the higher organic matter concentrations and longer exposure time there (22). Next, examine the effect of sulfate reduction on the carbonate system and therefore on atmospheric $p\text{CO}_2$ (schematically shown on the right side of Fig. 2). If the induced reduction in aerobic remineralization is exactly balanced by anoxic remineralization via sulfate reduction, there is no net change in remineralization, and the scenario is effectively described by reaction 2a minus reaction 1,

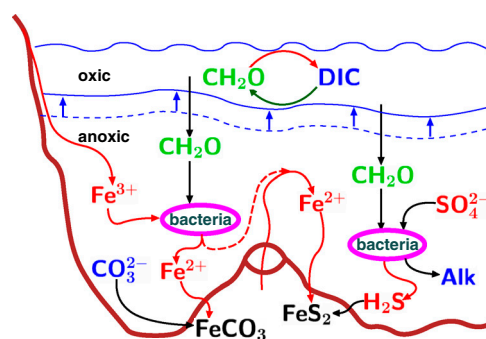
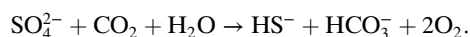


Fig. 2. Schematic of the biologically induced snowball initiation scenarios. The right side represents the sulfate reduction plus pyrite formation pathway, which increases alkalinity and therefore reduces $p\text{CO}_2$; the left side represents the iron reduction path, which leads to the deposition of siderite and reduction in the size of the DIC pool, and therefore, again, to the reduction of $p\text{CO}_2$. Note the shoaling of the (dashed blue) interface between the anoxic and oxic ocean depth ranges, in response to the enhanced export production, potentially leading to a reduction of both oxygenic production and aerobic remineralization. These scenarios are demonstrated using a single box model described in the text.

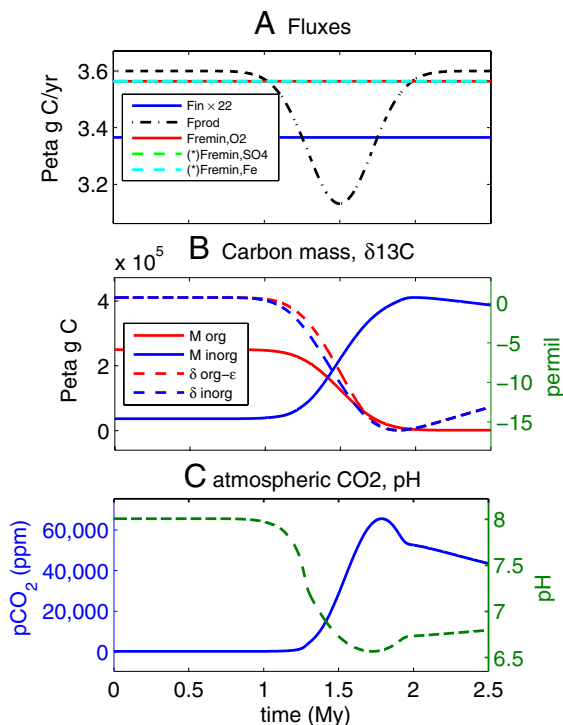


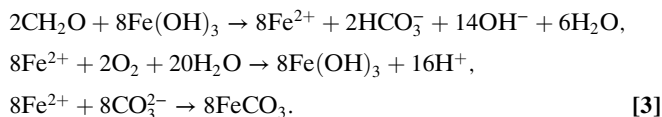
Fig. 1. Time-dependent results of scenario #1, a net aerobic remineralization of organic matter leading to a negative $\delta^{13}\text{C}$ isotopic excursion. Time advances from left to right. (A) Prescribed carbon fluxes; the only flux prescribed to change in this scenario is the decreasing oxygenic production F_{prod} forcing the isotopic signal. (*) Anaerobic remineralization fluxes are plotted shifted and are identically zero in this scenario. (B) Dissolved organic and inorganic carbon masses (solid lines) and $\delta^{13}\text{C}$ isotopic compositions (dashed). (C) Atmospheric $p\text{CO}_2$ (ppm) showing a large increase, due to the increase in dissolved inorganic carbon concentration, and a decrease in ocean pH.

Thus, the net reaction involves no change to the organic (CH_2O) or inorganic (CO_2 , HCO_3^-) carbon pools, but leads to a significant addition of carbonate alkalinity via the addition of HCO_3^- . Alkalinity may be defined as net charge due to ions of weak acids involved in the carbonate system; a useful approximation for the purpose of this section is $\text{Alk} = [\text{HCO}_3^-] + 2[\text{CO}_3^{2-}] + [\text{OH}^-] - [\text{H}^+]$; see *Materials and Methods* for details). An interesting consequence of the above scenario is that the added alkalinity leads to a reduction of the atmospheric pCO_2 (23), which may provide a biological mechanism for snowball initiation.

In order for a negative isotopic excursion to develop as well, a net remineralization of isotopically light organic matter is required, due to either increased remineralization rates or a drop in oxygenic production. This is a fine balance, as the net remineralization adds to the DIC pool and therefore tends to increase the pCO_2 . For a reduction in atmospheric pCO_2 to accompany an isotopic signal, the increase in alkalinity due to anaerobic remineralization must exceed the increase in the size of the DIC pool. This is demonstrated using specific time-dependent model scenarios in the next section.

If the sulfide (H_2S) formed by sulfate reduction within the sediments diffuses upward into the oxygenated ocean water, and is oxidized via reaction 2b, the carbonate alkalinity gained by sulfate reduction is lost and there is no reduction in atmospheric CO_2 . However, if the sulfide reacts with Fe^{2+} to form pyrite via reaction 2c within the sediments or within anoxic subsurface water masses, the alkalinity is retained. Below, we assume that 50% of the sulfide generated by bacterial sulfate reduction is removed by pyrite formation and that the rest is oxidized. Note that pyrite formation is a complex multistage process that is not completely understood. Arguments have been raised for (24–26) and against (27, 28) the reaction 2c used above, which is the net reaction of a complex multistage process. The *SI Appendix, section SI-3*, cites literature suggesting that this net reaction is a viable path in the presence of biological catalysts. Alternative pyrite formation scenarios to [2c] may lead to the removal of alkalinity added during sulfate reduction and eliminate the pCO_2 reduction (*SI Appendix, section SI-3*).

Next, consider a similar scenario involving anoxic remineralization of exported organic matter into DIC by iron-respiring bacteria reducing Fe^{3+} to Fe^{2+} . This reaction may again be followed by either mixing of Fe^{2+} toward the upper ocean and its oxidation back into Fe^{3+} , or by siderite (FeCO_3) formation and burial. These three reactions are represented by



Dissimilatory iron reduction of organic matter [3a] leads to a large injection of sixteen carbonate alkalinity units (via the 14OH^- and 2HCO_3^- terms) per two units of remineralized organic matter—while increasing the DIC by only two (via 2HCO_3^-). This would lead to a reduction of pCO_2 , except that once the Fe^{2+} is oxidized to Fe^{3+} via [3b] or reacts with the carbonate ion to form siderite via [3c], the entire alkalinity addition is lost. In the latter case, some DIC is deposited as siderite, which does lead to a reduction of pCO_2 .

Next, we consider specific model calculations based on the above scenarios. Although clearly not quantitative because of the many uncertainties regarding Neoproterozoic conditions, the results below are nonetheless useful in allowing us to visualize the above scenarios and examine their consequences.

Results of a Time-Dependent Scenario

The model is described in *Materials and Methods* and the *SI Appendix*. The results of the main scenario, involving both sulfate

and iron reduction, are summarized in Fig. 3. Fig. 3A shows the prescribed fluxes that drive the isotopic signal and atmospheric CO_2 drawdown. Export production is specified to increase over a time period of about 0.5 My, and then recover. In response, for the reasons explained above, both oxygenic primary production and aerobic remineralization are prescribed to decrease (dashed black and red curves). In parallel, exported organic matter is remineralized by sulfate reduction and iron reduction (dashed cyan and green).

The changes in productivity and remineralization fluxes correspond to a net remineralization, which leads to a decrease of the organic matter pool, which is converted to DIC (Fig. 3C). We find that we need to postulate a large initial organic matter pool (13), about 400 times larger than that of present day, to allow for a net remineralization event large enough to explain the observed isotopic signal. The net remineralization leads to a large isotopic excursion of DIC, 15‰ (Fig. 3C), and the isotopic compositions of the DOC covary with DIC as the latter is incorporated into newly produced DOC. This covariation is consistent with recent measurements of Neoproterozoic samples (14). Ref. 13 also assumed the DOC pool to be large, to prevent it from covarying with the DIC. This was motivated by earlier measurements indicating no such covariation (12). The carbonate system (Fig. 3B) responds to the changes in DIC, alkalinity fluxes, and enhanced DIC burial (below), leading to a significant CO_2 drawdown (Fig. 3I).

A major issue for the scenario considered here is the availability of sufficient sulfate and iron (see also ref. 29). Fig. 3D indicates that some 6 millimol per liter (mM) sulfate are needed, or, equivalently, that the maximum required sulfate flux into the ocean at the peak of the event be about four times the present-day flux. The Neoproterozoic ocean was most likely sulfate poor (30), with probably no more than about 10% of the present-day concentration of 28 mM. Recent arguments suggest higher sulfate concentrations can be maintained during ferruginous conditions (21), and are supported by sulfate evaporite deposition (31). A level of approximately 3 mM before the beginning of the event, supplemented by riverine continental flux about twice that of present day, could provide sufficient sulfate. Enhanced continental weathering due to continental collision and building of a supercontinent could provide the additional flux. Providing the implied Fe^{2+} flux for pyrite formation (solid blue curve in Fig. 3E, peaking at approximately 10×10^{12} mol/y) seems more of a challenge. Estimates of Fe^{2+} released today by midoceanic ridges vary between 2×10^{11} mol/y (32) and 9×10^8 mol/y (33). However, given the lower sulfate concentration in the Neoproterozoic, the hydrothermal Fe^{2+} concentration is expected to have been much higher (34). In addition, a somewhat higher-than-present Neoproterozoic heat flux could have led to a higher hydrothermal water flow, consistent with trace element measurements (35) that suggest a high ratio of hydrothermal to riverine input to the ocean in the late Proterozoic. The higher heat flux also implies higher temperatures in hydrothermal systems, which could lead to a hundredfold increase in the Fe^{2+} flux (36), bringing the required Fe^{2+} flux for pyrite formation within reach. The mechanisms suggested here for an increased Fe^{2+} supply to the ocean, although speculative, are consistent with iron speciation chemistry, which suggests that beginning about 800 My ago, anoxic subsurface waters were commonly ferruginous (20, 21). Finally, the required Fe^{3+} flux for iron reduction (solid red in Fig. 3E) peaks at (only) about 3 times present-day flux into the ocean (dashed red) and may result again from tectonically enhanced weathering associated with continental collision and building of a supercontinent (37). In addition, Fe^{3+} can accumulate in sediments before the beginning of the event and be used there by iron-reducing bacteria (38) during the event, so that the required amount of Fe^{3+} again does not seem to contradict existing information about iron availability.

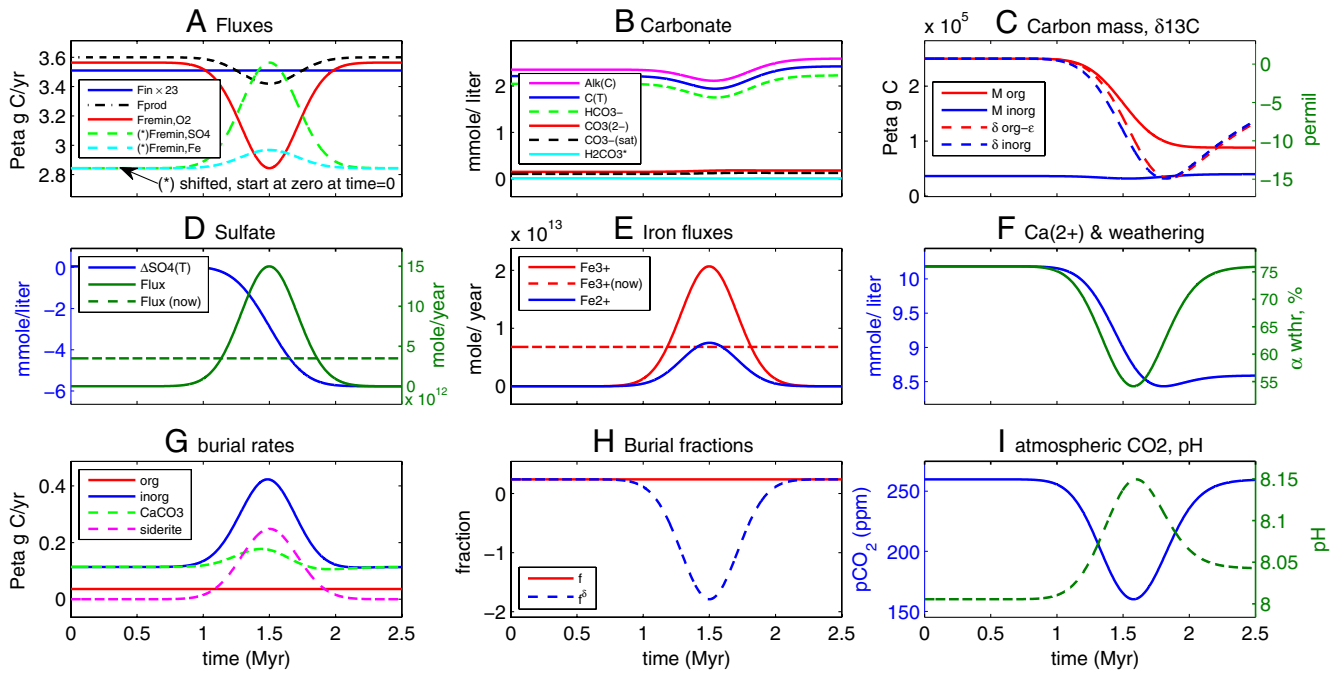


Fig. 3. Time-dependent model scenario (#2) of snowball initiation. (A) Prescribed carbon fluxes, due to oxygenic production (F_{prod}), aerobic remineralization ($F_{\text{remin},\text{O}_2}$), input from volcanoes and carbonate weathering (F_{in} , multiplied by 23), sulfate remineralization ($F_{\text{remin},\text{SO}_4}$) and iron reduction ($F_{\text{remin},\text{Fe}}$). (*) The last two fluxes, representing anaerobic remineralization, are plotted shifted and their initial value before the anomaly is zero. (B) Carbonate speciation. (C) Organic and inorganic carbon masses (solid lines) and $\delta^{13}\text{C}$ isotopic composition (dash). (D) Decrease in sulfate concentration $[\Delta\text{SO}_4(\text{T})]$, blue, or, alternatively, the required sulfate flux into the ocean (green, solid) for the sulfate reduction scenario. The present-day riverine flux is shown by the green, dashed line. (E) Implied iron fluxes of Fe^{3+} for iron reduction part of the scenario (red, with present-day flux into the ocean shown in red dashed line), and the implied flux of Fe^{2+} for the sulfate reduction and pyrite formation (blue). (F) Organic and inorganic burial rates. (G) Ca^{2+} and the weathering fraction α_{wthr} (SI Appendix). (H) Organic burial fraction f and non-steady-state fraction f^δ defined in the text. (I) Atmospheric CO_2 and ocean pH.

The low-latitude Neoproterozoic land mass distribution (39) could make the tropical oceans especially rich in iron and phosphate carried from the continents. Much of the biological production, anoxic remineralization, and exchange of CO_2 with the atmosphere may have therefore been concentrated in low-latitude seas. In this case, the relevant ocean volume participating in setting the atmospheric CO_2 could have been much smaller. The fluxes of iron and sulfate required to affect the carbonate system of this smaller ocean volume could be significantly reduced, making the scenario more realizable.

In aerobic scenarios of DOC remineralization, ocean pH decreases because of an increase in the size of the marine DIC pool, leading to enhanced dissolution of marine carbonates. The current scenario (Fig. 3G) predicts instead an increased rate of carbonate deposition during the isotopic excursion, due to increased alkalinity and pH. Intensified DIC burial, which disposes of the newly produced DIC and allows the drawdown of atmospheric CO_2 , is divided between deposition of calcium carbonate (with a corresponding decrease in Ca^{2+} concentration, Fig. 3F) and siderite.

The large isotopic signal found here is possible because of a deviation from steady-state dynamics (see a related discussion in ref. 13). If the DOC pool is not as large as assumed in ref. 13, it is likely in an isotopic quasi-equilibrium ($d\delta_{\text{org}}/dt \approx 0$) because of its short residence time. The isotopic compositions are then governed by (Materials and Methods) $\delta_{\text{org}} = \delta_{\text{inorg}} + \epsilon$ and

$$M_{\text{inorg}} \frac{d\delta_{\text{inorg}}}{dt} = F_{\text{in}}(\delta_{\text{in}} - \delta_{\text{inorg}}) - (F_{\text{prod}} - F_{\text{remin}})\epsilon, \quad [4]$$

where $\epsilon = -28\text{‰}$ is the fractionation between organic and inorganic matter, M_{inorg} is the DIC pool, F_{prod} is the organic matter production rate, F_{remin} is the total remineralization rate, F_{in} is the carbon flux from volcanoes and carbonate weathering, and δ_{in} is its isotopic composition. At the minimum point of an inorganic

isotopic excursion, where $\frac{d}{dt}\delta_{\text{inorg}} = 0$, we therefore have $\delta_{\text{inorg}} = \delta_{\text{in}} - f^\delta\epsilon$, with $f^\delta = (F_{\text{prod}} - F_{\text{remin}})/F_{\text{in}}$. In a steady state, $F_{\text{prod}} - F_{\text{remin}}$ is the organic burial rate and f^δ is then the organic burial fraction, f . But in a non-steady-state of the DIC pool, remineralization could significantly outpace primary production, making f^δ negative and large (Fig. 3H), leading to a large negative isotopic excursion (Fig. 3C) not possible in a steady state, when $f^\delta = f > 0$.

Fig. 3I shows the ocean pH increasing during the event, and the pCO_2 decreasing. Recent model estimates for the threshold CO_2 leading to a snowball vary from below present-day values to four times present-day values (40). We demonstrate that a pCO_2 reduction in conjunction with an appropriate isotopic signal is indeed possible under the specified scenario, and a much larger pCO_2 reduction is easily obtained by retuning the model. Given the enormous increase in pCO_2 in the standard aerobic remineralization scenario for explaining the isotopic signal (Fig. 1), it is remarkable that a self-consistent scenario invoking anaerobic remineralization can produce an isotopic excursion of as much as 15‰ as well as a significant decrease in pCO_2 (Fig. 3C and I). This provides a counterview to organic matter oxidation acting as a negative feedback preventing a full glaciation (41).

Carbon fluxes due to production and remineralization are prescribed rather than calculated from first principles here, because of uncertainties regarding Neoproterozoic biogeochemistry. We therefore consider in the SI Appendix, section SI-4, a fairly thorough set of sensitivity tests of our results to changes in prescribed fluxes, demonstrating the robustness of the model results to prescribed parameters.

Discussion and Comparison to Available Observations

This paper is motivated by a 200-My period of time, characterized by several major glacial events and isotope anomalies of distinct character. Given the simplicity of the model used here, it is best

not to attempt to model specific glaciations and isotopic anomalies found in the geologic record. Still, the scenario considered here may explain observed large negative presnowball $\delta^{13}\text{C}$ excursions, while accounting for a reduction in atmospheric pCO_2 that could lead to global glaciations. It also makes additional predictions that can be tested against the geologic record. Both the sulfate and iron reduction paths lead to an increased ocean pH (Fig. 3*I*). This modest pH increase represents an ocean-wide average, and could have been larger in some specific environments. Evidence of increased pH may be found in unusual centimeter-scale talc nodules formed during early diagenesis of carbonate sediments, observed to date only in mid-Neoproterozoic marine successions and requiring pore water $\text{pH} > 8.6$ (42). The increased pH also leads to a prediction of enhanced calcium carbonate deposition (Fig. 3*G*), consistent with the observation of widespread stromatolite formation in immediately preglacial successions (43). The model uncertainty does not allow us to determine whether the DIC deposition via siderite or carbonate precipitation may have dominated during the preglacial Neoproterozoic (Fig. 3*G*), yet both rates may be expected to be significant, in particular on anoxic continental shelves and slopes where organic carbon accumulates. Indeed shales deposited in anoxic shelf environments suggest that all deposited carbonates are siderite (a few percent of total deposits) (21), although it is difficult to estimate global budgets. We do not have a record of still deeper environments, and although preserved shallow-water environments show abundance of carbonate, they show little to no siderite, perhaps because they were oxygenated. Overall, geochemical observations of later Neoproterozoic sedimentary rocks seem consistent with the requirements and predictions of the scenario considered here.

Some recent observations show the large negative isotopic $\delta^{13}\text{C}$ excursions returning to positive values prior to the regional onset of glacial deposits (11, 18, 19). Moreover, the late Ediacaran Shuram anomaly is the largest in the geological record and appears to postdate the Neoproterozoic glaciations. This raises the interesting possibility that the $\delta^{13}\text{C}$ excursions and snowball events are not mechanistically linked. By changing the balance between iron reduction and sulfate reduction on one hand, and oxygenic production and aerobic remineralization on the other, the above scenario may be modified to result in a CO_2 reduction without a $\delta^{13}\text{C}$ signal, as well as an isotopic signal without CO_2 change (scenarios #5 and #6 in the *SI Appendix*, section SI-4; Figs. SI-5 and SI-6).

The oxygenic fixation of organic matter, followed by anaerobic remineralization, amounts to an oxygen source. The sulfide and iron oxidation act as oxygen sinks. The net oxygen source predicted here thus needs to be regulated by appropriate sinks so that the deep ocean remains anoxic for the above scenario to be valid. The implied O_2 source is significant, of the same order as present-day pyrite weathering and volcanogenic (via SO_2 gas) sink of O_2 (*SI Appendix*, section SI-5), seemingly allowing for the possibility of such regulation, except that weathering flux before the advent of land plants may have been as much as one order of magnitude weaker. All we can currently do is point out this significant difficulty with the scenario examined here.

Conclusions

We examined whether an enhanced export production scenario followed by anoxic remineralization of the sinking organic matter may lead to isotopic excursions as observed before the two largest Neoproterozoic glaciations. Specifically, sulfate reduction followed by pyrite formation increases alkalinity and therefore enhances calcium carbonate precipitation. Alkalinity gained during iron reduction is lost during the siderite formation that follows, but siderite formation itself leads to DIC burial. In both cases, and unlike the explanation of the isotopic signal via aerobic remineralization, the net effect can lead to a drawdown rather than a large increase of

atmospheric pCO_2 , possibly explaining both the isotopic signal and snowball initiation. Previously proposed mechanisms for ice age initiation (see the Introduction) may all supplement the scenario discussed here and are not inconsistent with it.

The factors that could lead to enhanced export production, and thus initiate the above scenario, remain conjectural. It is interesting to note, however, that although eukaryotes originated early in the Proterozoic Eon, if not earlier, both fossils (44) and molecular biomarkers (45) show evidence of dramatic increase in the abundance, diversity, and environmental distribution of marine eukaryotes beginning about 800 My ago. Biogeochemical consequences potentially include higher sinking rates on continental shelves, associated with larger mean cell size and propensity to form particulate aggregates (46); higher sinking rates associated with mineralized tests and scales (45, 47); and increased biomass associated with high (relative to cyanobacteria) C:N in eukaryotic phytoplankton (48). Thus, mid-Neoproterozoic increase in the importance of marine eukaryotes could have provided marine ecosystems with an unprecedented capacity for episodic increases in export flux. Therefore, given the increased vulnerability of the Earth system to glaciation introduced by tectonic factors, episodically enhanced increase in the export of organic matter into anoxic subsurface water masses and sediments could have pushed climate beyond the threshold for glaciations, and done so repeatedly. If later Ediacaran oceans were more broadly oxygenated (49), the biological mechanism introduced here for glacial initiation would no longer apply. The anaerobic remineralization mechanism considered here may be relevant to other carbon isotopic excursions in Earth history that did not necessarily involve the large pCO_2 increases expected from large-scale aerobic remineralization events. Although hypothetical and speculative, many aspects of the mechanisms considered here are testable, and it should be interesting to examine the geologic record in view of these ideas.

Materials and Methods

The model considers the ocean as a single volume, yet treats separately anoxic and oxic remineralization processes. The organic carbon mass (particulate and dissolved) is affected by primary production, total remineralization and burial, $dM_{\text{org}}/dt = F_{\text{prod}} - F_{\text{rem}} - F_{\text{b,org}}$, whereas the inorganic carbon mass is affected in addition by volcanic input, $dM_{\text{inorg}}/dt = F_{\text{in}} + F_{\text{remin}} - F_{\text{prod}} - F_{\text{b,inorg}}$. The organic and inorganic isotopic compositions are governed by $M_{\text{org}}d\delta_{\text{org}}/dt = F_{\text{prod}}(\delta_{\text{inorg}} + \varepsilon - \delta_{\text{org}})$ and $M_{\text{inorg}}d\delta_{\text{inorg}}/dt = F_{\text{in}}(\delta_{\text{in}} - \delta_{\text{inorg}}) - (F_{\text{prod}} - F_{\text{remin}})\varepsilon - F_{\text{remin}}(\delta_{\text{inorg}} + \varepsilon - \delta_{\text{org}})$, where ε represents the fractionation during biological production. The model includes an expanded carbonate system with the carbonate species, $\text{CO}_2(\text{g}) \rightleftharpoons \text{H}_2\text{CO}_3^*$, $\text{H}_2\text{O} \rightleftharpoons \text{H}^+ + \text{OH}^-$, $\text{H}_2\text{CO}_3^* \rightleftharpoons \text{H}^+ + \text{HCO}_3^-$, $\text{HCO}_3^- \rightleftharpoons \text{H}^+ + \text{CO}_3^{2-}$; boron, $\text{B}(\text{OH})_3 + \text{H}_2\text{O} \rightleftharpoons \text{H}^+ + \text{B}(\text{OH})_4^-$; sulfate and sulfide, $\text{HSO}_4^- \rightleftharpoons \text{H}^+ + \text{SO}_4^{2-}$, $\text{H}_2\text{S}(\text{aq}) \rightleftharpoons \text{HS}^- + \text{H}^+$. These are solved for at every time step to round-off accuracy using Jacobian-assisted optimization (*SI Appendix*, section SI-2.10), and given the values of total dissolved CO_2 , boron, sulfide, and sulfate and a generalized alkalinity (charge balance), all defined as follows, $C_T = [\text{H}_2\text{CO}_3^*] + [\text{HCO}_3^-] + [\text{CO}_3^{2-}]$, $B_T = [\text{B}(\text{OH})_4^-] + [\text{B}(\text{OH})_3]$, $S_T = [\text{HSO}_4^-] + [\text{SO}_4^{2-}]$, $(\text{H}_2\text{S})_T = [\text{H}_2\text{S}(\text{aq})] + [\text{HS}^-]$, $\text{Alk}_G = [\text{HCO}_3^-] + 2[\text{CO}_3^{2-}] + [\text{B}(\text{OH})_4^-] + [\text{HSO}_4^-] + 2[\text{SO}_4^{2-}] + [\text{HS}^-] + [\text{OH}^-] - [\text{H}^+]$. The total CO_2 is given by the inorganic carbon mass M_{inorg} per liter; total boron is specified at 400 $\mu\text{mol/L}$; total sulfide and sulfate concentrations are affected by sulfate remineralization flux, by the mixing of sulfide toward upper ocean and its eventual oxidation back to sulfate, and by pyrite formation, $d(\text{H}_2\text{S})_T/dt = +\frac{1}{2}F_{\text{remin,SO}_4} - F_{\text{H}_2\text{S,mixing}} - F_{\text{pyrite}}$, $dS_T/dt = -0.5F_{\text{remin,SO}_4} + F_{\text{H}_2\text{S,mixing}}$. Generalized alkalinity sources and sinks include the input weathering flux of calcium carbonate, inorganic burial, pyrite formation, iron remineralization, and mixing followed by oxidation of iron and siderite formation, $d\text{Alk}_G/dt = 2 \times \alpha_{\text{wthr}}F_{\text{in}} - 2 \times F_{\text{b,inorg}} - F_{\text{pyrite}} + 8F_{\text{remin,Fe}} - 2F_{\text{Fe,mixing}} - 2F_{\text{siderite}}$. The effect of the weathering feedback on alkalinity input, α_{wthr} , follows ref. 50. The calcium ion concentration is affected by input weathering flux and sedimentation/dissolution of CaCO_3 , $d\text{Ca}^{2+}/dt = F_{\text{in,Ca}^{2+}} - F_{\text{b,inorg}}$. Iron(III) is consumed by iron remineralization and produced by mixing and oxidation of iron(II), $d\text{Fe}^{3+}/dt = -4F_{\text{remin,Fe}} + F_{\text{Fe,mixing}}$. Iron(II) budget is additionally affected by siderite formation, $d\text{Fe}^{2+}/dt = 4F_{\text{remin,Fe}} - F_{\text{siderite}}$.

$F_{\text{Fe,mixing}}$. The prescribed fluxes have a Gaussian structure in time (*SI Appendix, section SI-2.2*). The response to step-forcing is examined in the *SI Appendix*, where the model is also fully described, and the response amplitude is found to be remarkably robust, although its temporal structure does depend on that of the forcing. The model code is written in Matlab and is available with the *SI Appendix* or at www.seas.harvard.edu/climate/eli/Downloads.

ACKNOWLEDGMENTS. We thank Timothy Lyons, Chris Reinhard, and two anonymous reviewers for most constructive and helpful comments. We are grateful for helpful discussions and comments from Arren Bar-Even, Don Canfield, Hezi Gildor, Peter Huybers, Francis Macdonald, Ron Milo, and Aldo Shemesh. This work was supported by National Science Foundation Grant ATM-0902844 (to E.T.) and National Aeronautics and Space Administration Grant NNX07AV51 (to A.H.K. and D.T.J.). E.T. thanks the Weizmann Institute for its hospitality during parts of this work.

- Harland WB (1964) *Problems in Palaeoclimatology*, ed AEM Nairn (John Wiley & Sons, London), pp 119–149 pp 180–184.
- Kirschvink J (1992) *The Proterozoic Biosphere: A Multidisciplinary Study*, eds J Schopf and C Klein (Cambridge Univ Press, Cambridge, U.K.), pp 51–52.
- Hoffman PF, Kaufman AJ, Halverson GP, Schrag DP (1998) A Neoproterozoic snowball Earth. *Science* 281:1342–1346.
- Schrag DP, Berner RA, Hoffman PF, Halverson GP (2002) On the initiation of a snowball Earth. *Geochem Geophys Geosyst* 3:1036.
- Knoll AH (1992) *The Origin and Early Evolution of Metazoans*, ed JL Signor P (Plenum, New York), pp 53–84.
- Godderis Y, et al. (2007) Coupled modeling of global carbon cycle and climate in the Neoproterozoic: Links between Rodinia breakup and major glaciations. *C R Geosci*, pp:212–222.
- Knoll AH, Hayes JM, Kaufman AJ, Swett K, Lambert IB (1986) Secular variation in carbon isotope ratios from upper Proterozoic successions of Svalbard and East Greenland. *Nature* 321:832–838.
- Halverson GP, Wade BP, Hurtgen MT, Barovich KM (2010) Neoproterozoic chemostratigraphy. *Precambrian Res* 182:337–350.
- Halverson GP, Hoffman PF, Schrag DP, Kaufman AJ (2002) A major perturbation of the carbon cycle before the Ghaub glaciation (Neoproterozoic) in Namibia: Prelude to snowball Earth? *Geochem Geophys Geosyst* 3:1035.
- Kaufman AJ, Knoll AH, Narbonne GM (1997) Isotopes, ice ages, and terminal Proterozoic Earth history. *Proc Natl Acad Sci USA* 94:6600–6605.
- Swanson-Hysell NL, et al. (2010) Cryogenian glaciation and the onset of carbon-isotope decoupling. *Science* 328:608–611.
- Hayes JM, Strauss H, Kaufman AJ (1999) The abundance of C-13 in marine organic matter and isotopic fractionation in the global biogeochemical cycle of carbon during the past 800 Ma. *Chem Geol* 161:103–125.
- Rothman DH, Hayes JM, Summons RE (2003) Dynamics of the Neoproterozoic carbon cycle. *Proc Natl Acad Sci USA* 100:8124–8129.
- Johnston DT, et al. (2010) New insight into the character of the Neoproterozoic carbon cycle. *Geological Society of America Abstracts with Programs* 42:395.
- Derry LA (2010) A burial diagenesis origin for the Ediacaran Shuram-Wonoka carbon isotope anomaly. *Earth Planet Sci Lett* 294:152–162.
- Knauth LP, Kennedy MJ (2009) The late Precambrian greening of the Earth. *Nature* 460:728–732.
- Swart PK, Kennedy M (2010) A comparison of the Trezona carbon anomaly with the Plio-Pleistocene. *Geological Society of America Abstracts with Programs* 42:396.
- Macdonald FA, Jones DS, Schrag DP (2009) Stratigraphic and tectonic implications of a newly discovered glacial diamictite-cap carbonate couplet in southwestern Mongolia. *Geology* 37:123–126.
- Macdonald FA, et al. (2010) Calibrating the Cryogenian. *Science* 327:1241–1243.
- Canfield D, et al. (2008) Ferruginous conditions dominated later Neoproterozoic deep water chemistry. *Science* 321:949–952.
- Johnston DT, et al. (2010) An emerging picture of Neoproterozoic ocean chemistry: Insights from the Chuar Group, Grand Canyon, USA. *Earth Planet Sci Lett* 290:64–73.
- Neretin LN, Bottcher ME, Grinenko VA (2003) Sulfur isotope geochemistry of the Black Sea water column. *Chem Geol* 200:59–69.
- Zeebe R, Wolf-Gladrow D (2001) *CO₂ in Seawater: Equilibrium, Kinetics, Isotopes*, (Elsevier, Amsterdam), Elsevier Oceanography Series, Vol. 65.
- Rickard D, Luther GW, III (2007) Chemistry of iron sulfides. *Chem Rev* 107:514–562.
- Drobner E, Huber H, Wachtershauser G, Rose D, Stetter KO (1990) Pyrite formation linked with hydrogen evolution under anaerobic conditions. *Nature* 346:742–744.
- Donald R, Southam G (1999) Low temperature anaerobic bacterial diagenesis of ferrous monosulfide to pyrite. *Geochim Cosmochim Acta* 63:2019–2023.
- Berner RA (1970) Sedimentary pyrite formation. *Am J Sci* 268:1–23.
- Benning LG, Wilkin RT, Barnes HL (2000) Reaction pathways in the Fe-S system below 100 degrees C. *Chem Geol* 167:25–51.
- Bristow TF, Kennedy MJ (2008) Carbon isotope excursions and the oxidant budget of the Ediacaran atmosphere and ocean. *Geology* 36:863–866.
- Hurtgen MT, Arthur MA, Suits NS, Kaufman AJ (2002) The sulfur isotopic composition of Neoproterozoic seawater sulfate: Implications for a snowball Earth? *Earth Planet Sci Lett* 203:413–429.
- Rainbird RH, Jefferson CW, Young GM (1996) The early Neoproterozoic sedimentary succession B of northwestern Laurentia: Correlations and paleogeographic significance. *Geol Soc Am Bull* 108:454–470.
- Elderfield H, Schultz A (1996) Mid-ocean ridge hydrothermal fluxes and the chemical composition of the ocean. *Annu Rev Earth Planet Sci* 24:191–224.
- Tagliabue A, et al. (2010) Hydrothermal contribution to the oceanic dissolved iron inventory. *Nat Geosci* 3:252–256.
- Kump LR, Seyfried WE (2005) Hydrothermal Fe fluxes during the Precambrian: Effect of low oceanic sulfate concentrations and low hydrostatic pressure on the composition of black smokers. *Earth Planet Sci Lett* 235:654–662.
- Derry L, Jacobsen S (1988) The Nd and Sr isotopic evolution of Proterozoic seawater. *Geophys Res Lett* 15:397–400.
- Seyfried WE, Janecky DR (1985) Heavy-metal and sulfur transport during subcritical and supercritical hydrothermal alteration of basalt—influence of fluid pressure and basalt composition and crystallinity. *Geochim Cosmochim Acta* 49:2545–2560.
- Tosca NJ, et al. (2010) Clay mineralogy, organic carbon burial, and redox evolution in Proterozoic oceans. *Geochim Cosmochim Acta* 74:1579–1592.
- Dong H, Jaisi DP, Kim J, Zhang G (2009) Microbe-clay mineral interactions. *Am Mineral* 94:1505–1519.
- Hoffman PF, Li ZX (2009) A palaeogeographic context for Neoproterozoic glaciation. *Palaeogeogr Palaeoclimatol Palaeoecol* 277:158–172.
- Voigt A, Abbot DS, Pierrehumbert RT, Marotzke J (2010) Initiation of a Marinoan snowball Earth in a state-of-the-art atmosphere-ocean general circulation model. *Clim Past Discuss* 6:1853–1894.
- Peltier WR, Liu Y, Crowley JW (2007) Snowball earth prevention by dissolved organic carbon remineralization. *Nature* 450 813-U1.
- Tosca NJ, Macdonald FA, Strauss JV, Johnston DT, Knoll AH (2011) Sedimentary talc in Neoproterozoic carbonate successions. *Earth Planet Sci Lett* 306:11–22.
- Hoffman PF (2011) Strange bedfellows: Glacial diamictite and cap carbonate from the Marinoan (635) glaciation in Namibia. *Sedimentology* 58:57–119.
- Knoll AH, Javaux E, Hewitt D, Cohen P (2006) Eukaryotic organisms in Proterozoic oceans. *Philos Trans R Soc Lond B Biol Sci* 361B:1023–1038.
- Cohen PA, Schopf JW, Butterfield NJ, Kudryavtsev AB, Macdonald FA (2011) Phosphate biomineralization in mid-Neoproterozoic protists. *Geology* 39:539–542.
- Burd AB, Jackson GA (2009) Particle aggregation. *Ann Rev Mar Sci* 1:65–90.
- Porter SM, Knoll AH (2000) Testate amoebae in the Neoproterozoic era: Evidence from vase-shaped microfossils in the Chuar Group, Grand Canyon. *Paleobiology* 26:360–385.
- Nagy RM, Porter SM, Dehler CM, Shen Y (2009) Biotic turnover driven by eutrophication before the Sturtian low-latitude glaciation. *Nat Geosci* 2:414–417.
- Canfield DE, Poulton SW, Narbonne GM (2007) Late-Neoproterozoic deep-ocean oxygenation and the rise of animal life. *Science* 315:92–95.
- Berner R (1994) GEOCARB-II—A revised model of atmospheric CO₂ over Phanerozoic time. *Am J Sci* 294:56–91.